An Amorphous Carbon Nitride Composite Derived from ZIF-8 as Anode Material for Sodium-Ion Batteries

Jing-Min Fan,[a, b] Jia-Jia Chen,[a, b] Qian Zhang,[a, b] Bin-Bin Chen,[a, b] Jun Zang,[a, b] Ming-Sen Zheng,*[a, b, c] and Quan-Feng Dong*[a, b, c]

An composite comprising amorphous carbon nitride (ACN) and zinc oxide is derived from ZIF-8 by pyrolysis. The composite is a promising anode material for sodium-ion batteries. The nitrogen content of the ACN composite is as high as 20.4%, and the bonding state of nitrogen is mostly pyridinic, as determined by X-ray photoelectron spectroscopy (XPS). The composite exhibits an excellent Na^+ storage performance with a reversible capacity of 430 $mAhg^{-1}$ and 146 $mAhg^{-1}$ at current densities of 83 mAg^{-1} and 8.33 Ag^{-1}, respectively. A specific capacity of 175 $mAhg^{-1}$ was maintained after 2000 cycles at 1.67 Ag^{-1}, with only 0.016% capacity degradation per cycle. Moreover, an accelerating rate calorimetry (ARC) test demonstrates the excellent thermal stability of the composite, with a low self heating rate and high onset temperature (210 °C). These results shows its promise as a candidate material for high-capacity, high-rate anodes for sodium-ion batteries.

Over the past several decades, the increasing consumption of fossil fuels in vehicles and thermal power plants has caused a severe energy crisis and environmental pollution. Clean sources of energy, such as solar and wind power, are considered as the most promising substitutes, but their irregular energy output requires energy storage systems that are safe, cheap, and easy to manage, and that can offer long cycle life.[1] Rechargeable lithium-ion batteries (LIBs) have been successfully applied in consumer electronics and electric vehicles because of their high energy density. Nonetheless, concerns have been raised about the future availability of lithium and, hence, its future cost, especially in light of the projected orders-of-magnitude increase in lithium usage for batteries in electric vehicles and smart grids.[2] In addition, there are safety issues associated with the formation of metal dendrites on the negative electrode.[3]

Owing to their low cost and the abundance of sodium, sodium-ion batteries (SIBs) are among the most promising alternatives to LIBs, especially for applications where gravimetric energy density is not a primary concern. Unfortunately, sodium-ion storage materials are rare in comparison to lithium-ion storage materials, especially for anodes,[4] because Na^+ has a much larger ionic radius (1.02 Å) than Li^+ (0.76 Å). This larger radius frustrates the movement of Na^+ in the host materials commonly explored as electrodes in LIBs.[5] Graphite, the most successful anode material for LIBs, exhibits an ultralow capacity for Na^+ insertion and sluggish diffusion kinetics.[6] Carbon materials with larger distances between their carbon atoms, such as expanded graphite,[7] hollow carbon nanowires,[8] porous carbons,[9] carbon fibres,[10] and graphene materials,[11] have demonstrated good battery performance, with reversible capacities of more than 280 $mAhg^{-1}$ and acceptable cycling stability. However, serious safety concerns also arise due to the possible formation of sodium dendrites in these anode materials, which have very low charge plateaus (between 0 and 0.1 V versus Na/Na^+), and the associated thermal runaway due to the low melting point of metallic sodium (98 °C).

Meanwhile, several studies have reported alloy anodes that employ metals with high specific capacities, such as germanium,[12] tin,[13] and antimony.[14] These alloys still suffer from poor cycling performance owing to large volume changes or sluggish kinetics. Several anode materials based on conversion chemistry (e.g., P,[15] MoS_2,[16] Sn_4P_3,[17] SnS_2,[18] and Sb_2S_3[19]) also exhibit high reversible capacities at appropriately low redox potentials. However, to overcome the poor electrical conductivity of these materials large amounts of carbon or of a conductive matrix have to be used to enhance their electrical conductivities. For example, phosphorus can deliver a theoretical specific capacity of 2596 $mAhg^{-1}$, which is probably the highest value among all known materials and several times higher than those of above-mentioned sodium alloys. However, phosphorus is unstable and using large amounts of carbon (ca. 30 wt%) in phosphorus/carbon composites greatly decreases the gravimetric and volumetric energy densities.[15] For materials dominated by the intercalation mechanism, such as spinel $Li_4Ti_5O_{12}$,[20] anatase TiO_2,[21] and P2-type layer materials,[22] an improved cycle life can be obtained but their specific capacity

[a] J.-M. Fan,+ J.-J. Chen,+ Q. Zhang,+ B.-B. Chen, J. Zang, M.-S. Zheng, Q.-F. Dong
State Key Laboratory of Physical Chemistry of Solid Surfaces
Xiamen University
Xiamen, Fujian, 361005 (PR China)
Fax: (+86) 0592-2183905
E-mail: qfdong@xmu.edu.cn
      mszheng@xmu.edu.cn

[b] J.-M. Fan,+ J.-J. Chen,+ Q. Zhang,+ B.-B. Chen, J. Zang, M.-S. Zheng, Q.-F. Dong
Department of Chemistry
Xiamen University
Xiamen, Fujian, 361005 (PR China)

[c] M.-S. Zheng, Q.-F. Dong
Collaborative Innovation Centre of Chemistry for Energy Materials
Xiamen University
Xiamen, Fujian, 361005 (PR China)

[+] These authors contributed equally to this work.

Supporting Information for this article is available on the WWW under http://dx.doi.org/10.1002/cssc.201500192.

is still limited, not higher than 200 mAh g^{-1}. Therefore, it is desirable to find new anode materials with high capacities and long cycling lifetimes, that also offer a high safety standard.

Herein, we report a porous amorphous carbon nitride (ACN) composite derived from zeolitic imidazolate frameworks 8 (ZIF-8) by a facile pyrolysis method. The composite exhibits excellent Na$^+$ storage performance and thermal stability when used as anode material in a sodium-ion battery. Benefitting from the unique stability and elastic recovery properties of carbon nitride, the ACN composite exhibits a stable and reversible Na$^+$ storage capacity of 430 mAh g^{-1}. Even at extremely high current densities of 8.33 A g^{-1}, it still delivers a reversible capacity of 140 mAh g^{-1}. Meanwhile, the ACN composite maintains a specific capacity of 175 mAh g^{-1} after 2000 cycles, with only 0.016 % capacity degradation per cycle. Moreover, the average discharge voltage is ca. 0.4 V vs. Na/Na$^+$, which not only ensures a high energy density when matched with suitable cathodes in fully rechargeable sodium-ion batteries, but also avoids the formation of sodium dendrites that cause serious safety issues.

Zeolitic imidazolate frameworks (ZIFs) are a subfamily of metal–organic frameworks (MOFs),[23] which have in the past decades been demonstrated to be among the most promising porous materials, with a wide range of applications in gas storage, gas separation, sensors, and other fields.[23a, 24] ZIF-8 is synthesized by copolymerization of Zn (II) with 2-methylimidazole links. We characterized the morphology of our as-prepared ZIF-8 and ACN composite by scanning electron microscopy (SEM) and transmission electron microscopy (TEM) (Figure 1a–d). A TEM image of the as-prepared ZIF-8 material shows that it is about 300 nm in size, with a uniform rhombic dodecahedral shape. After direct annealing of ZIF-8 under N$_2$ atmosphere the ACN composite maintained the morphology of ZIF-8 with 12 exposed {110} facets and a similar size (Figure 1b), demonstrating excellent structural stability. TEM and HRTEM images revealed that the ACN composite has a microporous structure and is amorphous. Powder X-ray diffraction (XRD) analysis confirmed the synthesis of ZIF-8 as a pure phase with good crystallinity (Figure 1e). The broad diffraction peaks at around 23°, 34°, and 44° suggest a low crystallinity for the ACN composite. To further investigate the porous structure of the ACN composite, N$_2$ adsorption–desorption analysis was performed at 77 K. These measurements revealed a type I Langmuir isotherm, and a Brunauer–Emmett–Teller (BET) surface area of 427 m^2 g^{-1}. The size of the micropores is less than 2 nm, as derived by using the Barrett–Joyner–Halenda (BJH) method (Figure 1 f; Supporting Information, Figure S1).

In earlier studies, materials derived from the pyrolysis of the ZIF-8 proved to be amorphous carbons with very low nitrogen content and almost zero zinc content, when the pyrolysis temperature is higher than 800 °C.[25] It is believed that the 2-methylimidazole ligand of ZIF-8 is carbonized during the pyrolysis process, while the nitrogen species and the zinc species are vaporized.[25a, b] However, the present ACN composite was pyrolysed at 700 °C and is a material with very high contents of nitrogen and zinc, showing extraordinary properties. Elemental analysis (C, H, N) revealed that the ACN composite contains
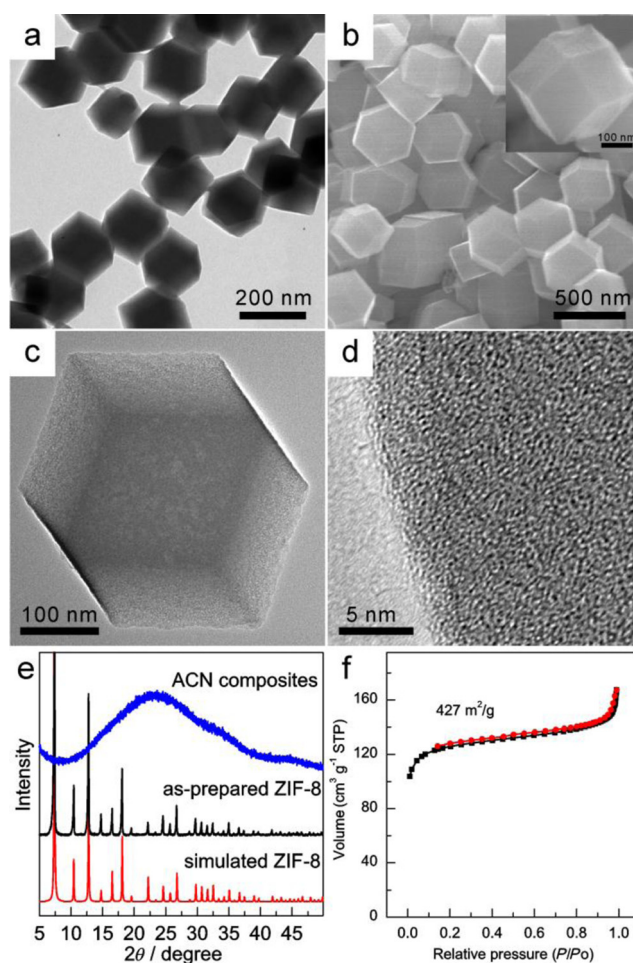

Figure 1. a) TEM image showing the morphology of as-prepared ZIF-8. b) SEM image of the ACN composite. c) Corresponding TEM image of ACN composite, and d) high-resolution TEM image (HRTEM). e) Powder X-ray diffraction patterns of simulated ZIF-8, as-prepared ZIF-8, and ACN composite. f) N$_2$ adsorption–desorption analysis of the ACN composite.

20.4 wt % N, 35.7 wt % C, and 2.2 wt % H (Supporting Information, Table S1). Thermo-gravimetric analysis (TGA; Supporting Information, Figure S2) showed a mass loss of 61.3 % under an O$_2$ atmosphere, which is close to the total content of C, H, and N. Considering that the zinc content of ZIF-8 is 28.6 %, the residual 38.7 % is likely ZnO. An X-ray photoelectron spectroscopy (XPS) survey demonstrated that the ACN composite contained the elements C, N, O, and Zn, and that the atomic ratio of Zn to O was close to 1:1 (Supporting Information, Figure S3). This is consistent with the TGA results. Likely, the Zn^{2+} species in the ZIF-8 were first reduced to metallic zinc in the N$_2$ atmosphere during the pyrolysis process, and then oxidized to ZnO when exposed to air after the pyrolysis. However, we did not detect patterns of ZnO by XRD (Figure 1e). This may be because of its ultrafine size or amorphous state in the composite, which is difficult to be detected by powder XRD. Dark-field TEM (Supporting Information, Figure S4) and high-resolution TEM (Figure 1d) also did not reveal obvious crystalline ZnO species in the ACN composite.
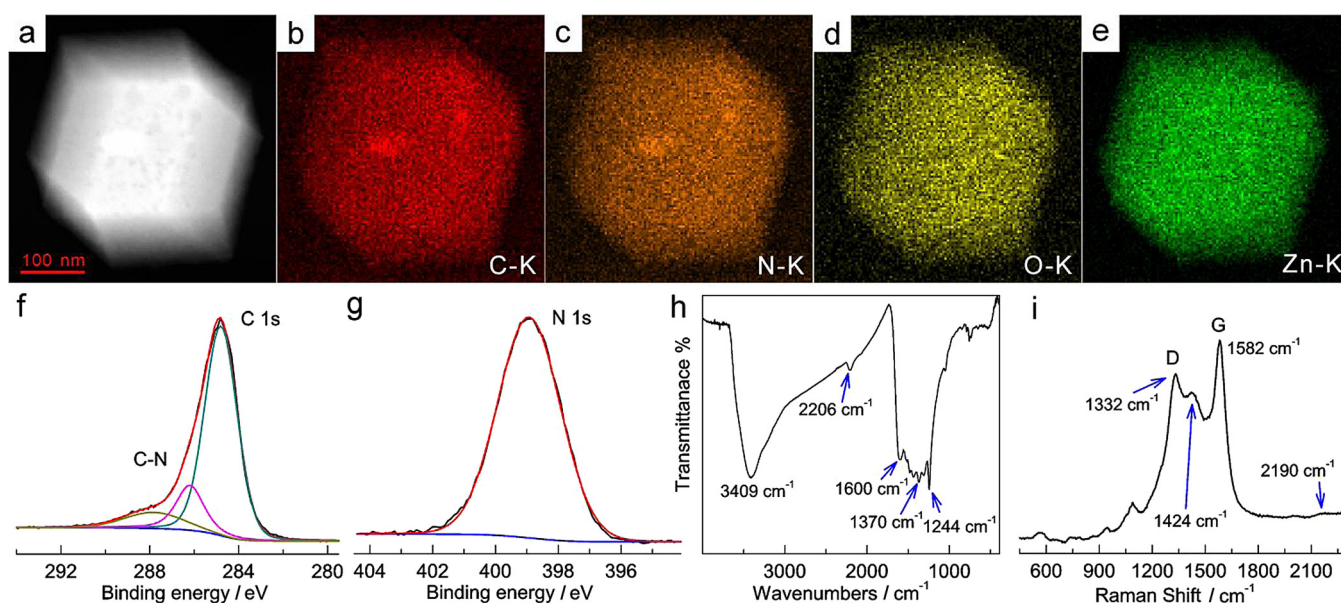
Figure 2. a–e) Energy-dispersive X-ray spectroscopy of C, N, O, and Zn. f, g) X-ray photoelectron spectroscopy (XPS) of C 1s and N 1s, respectively. The spectra are shown with raw data and fitting data derived by Lorentz–Gaussian function. h) FT-IR of the ACN composite. i) Raman spectrum, collected in the range of 1000–2300 cm^{-1} by using an excitation wavelength of 532 nm and duration of 40 s. Laser power: 1 mW.

Figure 2a shows a dark-field TEM image of the as-prepared ACN composite. The distribution of C, N, O, and Zn was determined by energy-dispersive X-ray spectroscopy (EDX) analysis. Figure 2b–e shows EDX mappings for C, N, O, and Zn, revealing that they are uniformly distributed throughout the ACN composite. To determine the chemistry of the carbon and nitrogen atoms in the ACN composite, we obtained X-ray photoelectron spectroscopy (XPS) measurements. The C 1s spectrum (Figure 2 f) shows a peak at around 284.8 eV, corresponding to sp^2 carbon, and peaks at 286.2 and 287.8 eV, assigned to C–N species.[26] Interestingly, the N 1s spectrum shows only one sharp and symmetric peak at 398.9 eV, which can be assigned to amorphous carbon nitride or pyridinic nitrogen (Figure 2 g).[27] No peaks are observed at 396 eV, which would correspond to Zn_3N_2,[28] indicating that the nitrogen atoms in the composite are fully bonded to carbon.

To obtain more detailed information on the nature of the C, N compounds in the ACN composite, we employed FT-IR and Raman spectroscopy. In the FT-IR spectrum of the ACN composite (Figure 2 h), a large broad band is visible at 3409 cm^{-1}, which can be assigned to stretching vibration modes of NH_2 and NH groups. Triazine-type absorption bands are observed in the range 1100–1600 cm^{-1}, and correspond to C–N and C=N stretching vibrations. The strong absorptions at 1244 and 1370 cm^{-1} are generally assigned to C–N vibrations of aromatic secondary and tertiary amines.[29] There is a little absorbance at 2206 cm^{-1}, confirming that minor C≡N or N=C=N components are generated during the carbonization process. The Raman spectrum of the ACN composite (Figure 2 i) agrees well with the FT-IR results. Generally, amorphous carbon has Raman-active G and D bands at around 1570 and 1360 cm^{-1} which correspond to the symmetric E_{2g} vibration mode in graphite-like materials and the disordered structure,

respectively.[30] However, there is a downward shift for the D band (1332 cm^{-1}) and an upward shift for the G band (1582 cm^{-1}). The downward shift of the D band can be attributed to a strained or curved graphite plane, which is caused by nitrogen atoms bonded to disordered carbon atoms (fourfold coordinated). The upward shift of the G band is an indication of graphitization (C=C, C=N), which indicates the crystallites are three-fold coordinated (sp^2 hybridization).[31] The Raman peak at 1424 cm^{-1} can be assigned to the N=N stretching mode in the form of C–N=N vibrations. The weak peak at 2190 cm^{-1} implies the existence of bonded C≡N groups, which only appears in amorphous carbon nitrides with a high nitrogen content.[32] We conclude that the ACN composite mainly comprises amorphous carbon nitride and zinc oxide.

Amorphous carbon nitride is an interesting material with good values for mechanical properties, such as hardness and elastic recovery, and good tribological properties,[33] resulting in excellent electrochemical stability. The electrochemical performance of the ACN composite as an anode material for sodium-ion battery was measured between 0.01–2.5 V vs. Na/Na^+. Figure 3a shows galvanostatic charge–discharge profiles of the ACN composite. The ACN composite can deliver an initial discharge capacity of 640 $mA\,h\,g^{-1}$ and a reversible capacity of 430 $mA\,h\,g^{-1}$ at a current density of 83 $mA\,g^{-1}$ with a Coulombic efficiency of 67.2%. The irreversible capacity during the 1st discharging/charging process should originate from the formation of a solid–electrolyte interphase (SEI) layer and a side reaction on the electrode/electrolyte interfaces,[8,9b] which is in good accordance with results obtained by cyclic voltammetry (CV) (Supporting Information, Figure S5). Notably, the insertion process of Na^+ ions into the ACN composite mostly occurs at average voltage of 0.4 V vs. Na/Na^+, which is a little higher than that for previous reported carbon materials (between 0
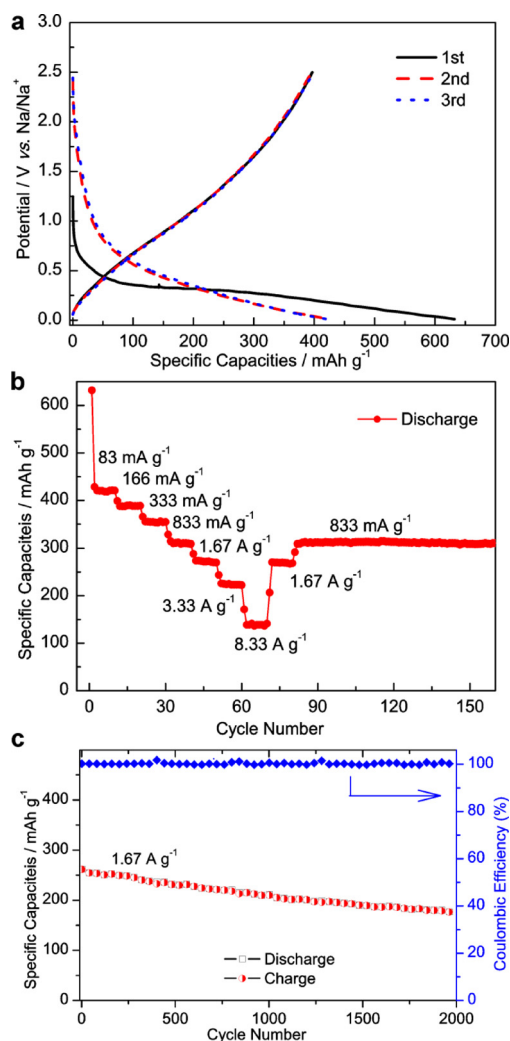
Figure 3. a) The first three discharge/charge curves of ACN composite obtained at 83 mA g^{-1}. After the activation process in the 1st cycle, the ACN composite exhibits stable and reversible Na$^+$ storage. Most Na$^+$ insertion occurs within the voltage window 0.8–0.01 V. b) Rate performance of the ACN composite at various current densities. c) Long-cycling testing of ACN composite at 1.67 A g^{-1} without 1st cycle of activation process. A specific capacity of 175 mA h g^{-1} was still retained after 2000 cycles and there was only 0.016% capacity degradation per cycle. All the specific capacities are based on the mass of ACN.

and 0.1 V versus Na$^+$/Na).[9] Such a working plateau will avoid the formation of sodium dendrites, which is the main cause of safety concerns. Meanwhile, it ensures an acceptable energy density, matching well with the cathodes to a fully rechargeable sodium ion battery. Moreover, the ACN composite also exhibits excellent rate capability and cycle stability as the anode for sodium ion batteries.

Figure 3 b shows the rate capability of the ACN composite. The ACN composite can deliver a reversible capacity of 430, 390, 360, 310, 270, and 220 mA h g^{-1} at current densities of 83, 166, 333, 833, 1670, and 3340 mA g^{-1}, respectively. Even at a very high current density of 8.33 A g^{-1}, a reversible capacity of 140 mA h g^{-1} is acquired. When the current density is lowered to 833 mA g^{-1}, the discharge capacity of the ACN composite can recover to 310 mA h g^{-1}, exhibiting excellent stability

in its rate performance. The cycling measurements was carried out at a current density of 1.67 A g^{-1}, as shown in Figure 3 c. The composite showed a capacity of 175 mA h g^{-1} after 2000 cycles, with only 0.016% capacity degradation per cycle and almost 100% Coulumbic efficiency.

To further investigate the ACN electrodes after charging and discharging, the electrodes in fully charged and discharged state were examined by SEM and XPS. As shown in Figure 4 a–c, an SEI film can be found in the ACN composite after charging/discharging processes, while no change is observed in the
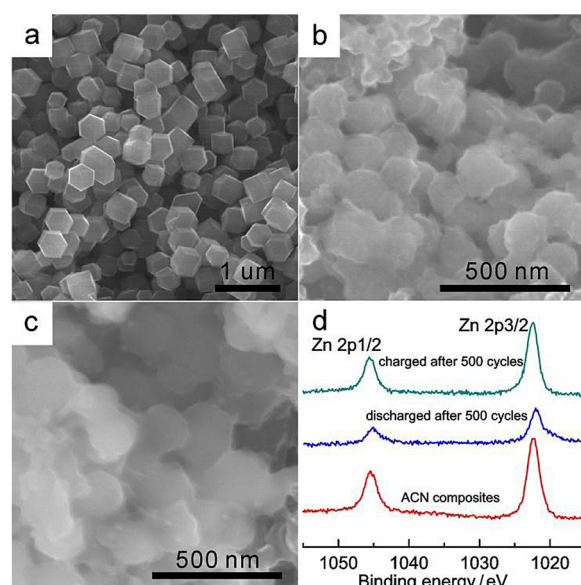

Figure 4. SEM images of a) ACN composite, b) ACN electrode after 500 cycles at fully charged state, and c) ACN electrode after 500 cycles at full discharge state. d) X-ray photoelectron spectroscopy (XPS) of Zn element in the ACN composite, discharged and charged after 500 cycles.

particle size and the morphology of the ACN composite after 500 cycles. Importantly, the size of the ACN composite particles in fully charged and discharged state are almost the same, which means that no major volume change occurs in the Na$^+$ ion insertion/extraction processes. This is likely due to its porous structure, and leads to the excellent cycling stability. Figure 4 d shows the XPS spectra of zinc for the composite in pristine and charged/discharged state after 500 cycles. The chemical state of ZnO in the three electrodes is the same, which means that the capacity of the ACN composite is due to the carbon nitride component (Supporting Information, Figure S6). To investigate the function of ZnO in the composite, the ACN composite was washed with 2 M HCl to remove it. Figure S7 (Supporting Information) shows the inferior cycling stability after ZnO removal compared to the ACN composite. The results imply that ZnO stabilizes the composite's structure. Thus, the excellent electrochemical performance of the ACN composite can be ascribed to the following: 1) The stable amorphous carbon nitride guarantees the high reversible capacity. 2) The microporous structure and large specific surface facilitates Na$^+$ and electron transfer at the electrode/electro-

lyte interfaces. 3) The presence of ultrafine ZnO particles maintains the rigid structure, leading to excellent cycling stability.

The thermal stability of the ACN composite in fully discharged state was evaluated in $NaPF_6$/EC:DEC electrolyte by using an accelerating rate calorimeter (ARC) at the temperature range of 80–360 °C under adiabatic conditions. According to an earlier study, the self-heating rate of hard carbon in $NaPF_6$/EC:DEC electrolyte is very high and the onset temperature is around 130 °C, which will easily result in a thermal runaway for a sodium ion battery.[34] Figure 5 shows the self-heating rate vs. T profile of the ACN composite in the fully charged sate. The
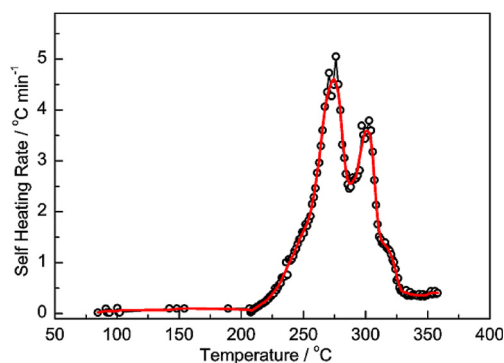

Figure 5. Thermal stability testing of the ACN composite in fully charged state by accelerated rate calorimetry (ARC) using $NaPF_6$/EC:DEC as electrolyte.

onset temperature of the ACN composite is around 210 °C, corresponding to the generation of sodium alkyl carbonates, while the self-heating rate of the ACN composite is always lower than 5.5 °C min^{-1} and reaches its peak at 260 °C. This result is superior to the reported thermostability of hard carbon in $NaPF_6$/EC:DEC electrolyte, and even better than the performance of Li/hard carbon in 1 M $LiPF_6$/EC:DEC electrolyte.[35]

In summary, we demonstrate a new type of amorphous carbon nitride (ACN) composite material derived from ZIF-8 that is a promising anode material for sodium-ion batteries. The ACN composite comprises carbon nitride and zinc oxide, and is synthesized by pyrolysis of ZIF-8 at 700 °C. Owing to the chemical nature of carbon nitride and stabilization by zinc oxide, the ACN composite offers excellent electrochemical performance. The composite shows a reversible capacity of 430 mAh g^{-1} at 83 mA g^{-1}, even 146 mAh g^{-1} under an extremely high current of 8.33 A g^{-1}. There is only 0.016% capacity degradation per cycle in 2000 cycles at a current density of 1.67 A g^{-1}, with a Coulombic efficiency of 100%. The ACN composite exhibits excellent thermal stability with a low self-heating rate (lower than 5.5 °C min^{-1}) and high onset temperature (210 °C), which shows its promise as anode material for future sodium-ion batteries.

Experimental Section

Materials synthesis: The ACN composite was synthesized by direct carbonization of ZIF-8 particles, which were prepared by using a modified method as following:[36] $Zn(NO_3)_2$ (734.4 mg) was dissolved into methanol (100 mL), and 2-methylimidazole (810.6 mg) was dissolved in methanol (100 mL) to generate a clear solution. The solutions were mixed and stirred for 5 min. The solution was aged at room temperature for 24 h. After that, white ZIF-8 powder precipitated. The ZIF-8 powder was collected by centrifugation, washed with methanol several times, and dried in an oven at 80 °C over night. The ZIF-8 powder was then directly heat-treated under nitrogen flow at 700 °C for 2 h at a heating rate of 5 °C min^{-1}.

Structural and physical characterization: The morphology of the as-prepared product was determined by scanning electron microscopy (SEM, HITACHI S-4800) and high-resolution transmission electron microscopy (HRTEM, F30). The specific surface area and average pore diameter were measured by static N_2 physisorption at 77 K on a Micromeritics TriStar II3020 surface area and pore analyzer. Powder X-ray diffraction (XRD) measurements were performed by using a Rigaku Ultima IV instrument using $Cu_{K\alpha}$ radiation ($\lambda = 0.15418$ nm). X-ray photoelectron spectroscopy (XPS) measurements were carried out on a XPS apparatus (PHI QUANTUM 2000) and elemental analysis was performed on Vario EL III. Raman spectra were collected by a Renishaw Raman microscope with an excitation wavelength of 532 nm.

Electrochemical measurements: The cathodes were prepared by mixing 80 wt% ACN composite, 10 wt% acetylene black, and 10 wt% water soluble polymer n-lauryl acrylate (LA, Chengdu, China). The resulting slurries were coated onto Cu foil current collectors and dried at 60 °C under vacuum overnight. A glass fibre filter was used as a separator and the electrolyte used was 1 M $NaPF_6$ dissolved in ethylene carbonate (EC) + diethyl carbonate (DEC) (47:47, v/v) with 6% fluorinated ethylene carbonate as an electrolyte additive. Metallic sodium was used as the anode. These components were sealed under Argon atmosphere into a CR2016-type coin cell. The galvanostatic charge–discharge testing was conducted on a NEWARE BTS-5V/5 mA type battery charger (Shenzhen NEWARE Co., China).

Thermal stability test: CR2016 coin cells were made and discharged to 0.01 V, and then the cells were opened in an argon-filled glove box and the electrode powder was rinsed with DEC four times and dried in the glove box. Typically, 50 mg discharged anode material and 0.5 mL electrolyte were used for the ARC tests (Accelerated Rate Calorimetry, North House, Bletchley, MK1 1SW, UK). Exothermic reactions were tracked under adiabatic conditions when the sample's self-heating rate exceeded 0.02 °C min^{-1}. ARC tests were stopped at 400 °C or when the exothermic process finished.

[1] a) M. Armand, J. M. Tarascon, *Nature* **2008**, *451*, 652; b) B. Dunn, H. Kamath, J.-M. Tarascon, *Science* **2011**, *334*, 928.

[2] a) X. Chen, C. Li, M. Gratzel, R. Kostecki, S. S. Mao, *Chem. Soc. Rev.* **2012**, *41*, 7909; b) J. B. Goodenough, K.-S. Park, *J. Am. Chem. Soc.* **2013**, *135*, 1167.

[3] H. Wu, D. Zhuo, D. Kong, Y. Cui, *Nat. Commun.* **2014**, *5*, 5193.

[4] J. Qian, Y. Xiong, Y. Cao, X. Ai, H. Yang, *Nano Lett.* **2014**, *14*, 1865.

[5] a) S.-W. Kim, D.-H. Seo, X. Ma, G. Ceder, K. Kang, *Adv. Energy Mater.* **2012**, *2*, 710; b) M. D. Slater, D. Kim, E. Lee, C. S. Johnson, *Adv. Funct. Mater.* **2013**, *23*, 947.

[6] M. M. Doeff, Y. Ma, S. J. Visco, L. C. De Jonghe, *J. Electrochem. Soc.* **1993**, *140*, L169.

[7] Y. Wen, K. He, Y. Zhu, F. Han, Y. Xu, I. Matsuda, Y. Ishii, J. Cumings, C. Wang, *Nat. Commun.* **2014**, *5*, 4033.

[8] Y. Cao, L. Xiao, M. L. Sushko, W. Wang, B. Schwenzer, J. Xiao, Z. Nie, L. V. Saraf, Z. Yang, J. Liu, *Nano Lett.* **2012**, *12*, 3783.

[9] a) R. Alcántara, P. Lavela, G. F. Ortiz, J. L. Tirado, *Electrochem. Solid-State Lett.* **2005**, *8*, A222; b) J. Ding, H. Wang, Z. Li, A. Kohandehghan, K. Cui, Z. Xu, B. Zahiri, X. Tan, E. M. Lotfabad, B. C. Olsen, D. Mitlin, *ACS Nano* **2013**, *7*, 11004; c) E. M. Lotfabad, J. Ding, K. Cui, A. Kohandehghan, W. P. Kalisvaart, M. Hazelton, D. Mitlin, *ACS Nano* **2014**, *8*, 7115.

[10] a) L. Fu, K. Tang, K. Song, P. A. van Aken, Y. Yu, J. Maier, *Nanoscale* **2014**, *6*, 1384; b) W. Li, L. Zeng, Z. Yang, L. Gu, J. Wang, X. Liu, J. Cheng, Y. Yu, *Nanoscale* **2014**, *6*, 693.

[11] Y. Yan, Y.-X. Yin, Y.-G. Guo, L.-J. Wan, *Adv. Energy Mater.* **2014**, *4*, 10.1002/aenm.201301584.

[12] K. H. Seng, M.-H. Park, Z. P. Guo, H. K. Liu, J. Cho, *Angew. Chem. Int. Ed.* **2012**, *51*, 5657; *Angew. Chem.* **2012**, *124*, 5755.

[13] Z. Zhu, S. Wang, J. Du, Q. Jin, T. Zhang, F. Cheng, J. Chen, *Nano Lett.* **2014**, *14*, 153.

[14] a) L. Wu, X. Hu, J. Qian, F. Pei, F. Wu, R. Mao, X. Ai, H. Yang, Y. Cao, *Energy Environ. Sci.* **2014**, *7*, 323; b) Y. Zhu, X. Han, Y. Xu, Y. Liu, S. Zheng, K. Xu, L. Hu, C. Wang, *ACS Nano* **2013**, *7*, 6378.

[15] a) Y. Kim, Y. Park, A. Choi, N.-S. Choi, J. Kim, J. Lee, J. H. Ryu, S. M. Oh, K. T. Lee, *Adv. Mater.* **2013**, *25*, 3045; b) J. Qian, X. Wu, Y. Cao, X. Ai, H. Yang, *Angew. Chem. Int. Ed.* **2013**, *52*, 4633; *Angew. Chem.* **2013**, *125*, 4731.

[16] a) Z. Hu, L. Wang, K. Zhang, J. Wang, F. Cheng, Z. Tao, J. Chen, *Angew. Chem. Int. Ed.* **2014**, *53*, 12794; *Angew. Chem.* **2014**, *126*, 13008; b) C. Zhu, X. Mu, P. A. van Aken, Y. Yu, J. Maier, *Angew. Chem. Int. Ed.* **2014**, *53*, 2152; *Angew. Chem.* **2014**, *126*, 2184.

[17] Y. Kim, Y. Kim, A. Choi, S. Woo, D. Mok, N.-S. Choi, Y. S. Jung, J. H. Ryu, S. M. Oh, K. T. Lee, *Adv. Mater.* **2014**, *26*, 4139.

[18] B. Qu, C. Ma, G. Ji, C. Xu, J. Xu, Y. S. Meng, T. Wang, J. Y. Lee, *Adv. Mater.* **2014**, *26*, 3854.

[19] D. Y. W. Yu, P. V. Prikhodchenko, C. W. Mason, S. K. Batabyal, J. Gun, S. Sladkevich, A. G. Medvedev, O. Lev, *Nat. Commun.* **2013**, *4*, 2922.

[20] Y. Sun, L. Zhao, H. Pan, X. Lu, L. Gu, Y.-S. Hu, H. Li, M. Armand, Y. Ikuhara, L. Chen, X. Huang, *Nat. Commun.* **2013**, *4*, 1870.

[21] K.-T. Kim, G. Ali, K. Y. Chung, C. S. Yoon, H. Yashiro, Y.-K. Sun, J. Lu, K. Amine, S.-T. Myung, *Nano Lett.* **2014**, *14*, 416.

[22] a) Y. Wang, X. Yu, S. Xu, J. Bai, R. Xiao, Y.-S. Hu, H. Li, X.-Q. Yang, L. Chen, X. Huang, *Nat. Commun.* **2013**, *4*, 2365; b) H. Yu, Y. Ren, D. Xiao, S. Guo, Y. Zhu, Y. Qian, L. Gu, H. Zhou, *Angew. Chem. Int. Ed.* **2014**, *53*, 8963; *Angew. Chem.* **2014**, *126*, 9109.

[23] a) R. Banerjee, A. Phan, B. Wang, C. Knobler, H. Furukawa, M. O'Keeffe, O. M. Yaghi, *Science* **2008**, *319*, 939; b) X.-C. Huang, Y.-Y. Lin, J.-P. Zhang, X.-M. Chen, *Angew. Chem. Int. Ed.* **2006**, *45*, 1557; *Angew. Chem.* **2006**, *118*, 1587.

[24] a) C.-H. Kuo, Y. Tang, L.-Y. Chou, B. T. Sneed, C. N. Brodsky, Z. Zhao, C.-K. Tsung, *J. Am. Chem. Soc.* **2012**, *134*, 14345; b) G. Lu, J. T. Hupp, *J. Am. Chem. Soc.* **2010**, *132*, 7832.

[25] a) W. Chaikittisilp, M. Hu, H. Wang, H.-S. Huang, T. Fujita, K. C. W. Wu, L.-C. Chen, Y. Yamauchi, K. Ariga, *Chem. Commun.* **2012**, *48*, 7259; b) H.-L. Jiang, B. Liu, Y.-Q. Lan, K. Kuratani, T. Akita, H. Shioyama, F. Zong, Q. Xu, *J. Am. Chem. Soc.* **2011**, *133*, 11854; c) H. B. Wu, S. Wei, L. Zhang, R. Xu, H. H. Hng, X. W. Lou, *Chem. Eur. J.* **2013**, *19*, 10804; d) F. Zheng, Y. Yang, Q. Chen, *Nat. Commun.* **2014**, *5*, 5261.

[26] a) Z. Sun, Z. Yan, J. Yao, E. Beitler, Y. Zhu, J. M. Tour, *Nature* **2010**, *468*, 549; b) D. Wei, Y. Liu, Y. Wang, H. Zhang, L. Huang, G. Yu, *Nano Lett.* **2009**, *9*, 1752.

[27] a) J. R. Pels, F. Kapteijn, J. A. Moulijn, Q. Zhu, K. M. Thomas, *Carbon* **1995**, *33*, 1641; b) J. M. Ripalda, E. Román, N. Díaz, L. Galán, I. Montero, G. Comelli, A. Baraldi, S. Lizzit, A. Goldoni, G. Paolucci, *Phys. Rev. B* **1999**, *60*, R3705.

[28] M. Futsuhara, K. Yoshioka, O. Takai, *Thin Solid Films* **1998**, *322*, 274.

[29] a) D. R. Miller, J. Wang, E. G. Gillan, *J. Mater. Chem.* **2002**, *12*, 2463; b) Y. Zhao, Z. Liu, W. Chu, L. Song, Z. Zhang, D. Yu, Y. Tian, S. Xie, L. Sun, *Adv. Mater.* **2008**, *20*, 1777.

[30] A. C. Ferrari, J. Robertson, *Philos. Trans. R. Soc. London Ser. A* **2004**, *362*, 2477.

[31] G.-Q. Yu, S.-H. Lee, J.-J. Lee, *Diamond Relat. Mater.* **2002**, *11*, 1633.

[32] A. K. M. S. Chowdhury, D. C. Cameron, M. S. J. Hashmi, *Thin Solid Films* **1998**, *332*, 62.

[33] A. Y. Liu, M. L. Cohen, *Science* **1989**, *245*, 841.

[34] X. Xia, J. R. Dahn, *J. Electrochem. Soc.* **2012**, *159*, A515.

[35] J. Jiang, J. R. Dahn, *Electrochim. Acta* **2004**, *49*, 4599.

[36] J. Cravillon, R. Nayuk, S. Springer, A. Feldhoff, K. Huber, M. Wiebcke, *Chem. Mater.* **2011**, *23*, 2130.